Developing Criteria and an Algorithm for Low-Cost IoT-Based Air Quality Sensor Network for Near-Road Air Quality Monitoring

Ram M. Magdaong[1], Ma. Rosario Concepcion O. Ang[1,2], John Richard E. Hizon[3], John Miguel A. Tutanes[1]

[1]Department of Geodetic Engineering, University of the Philippines Diliman, Quezon City, Philippines – {rmmagdaong, moang, jatutanes}@up.edu.ph
[2]Training Center for Applied Geodesy and Photogrammetry, University of the Philippines Diliman, Quezon City, Philippines
[3]Electrical and Electronics Engineering Institute, University of the Philippines Diliman, Quezon City, Philippines – richard.hizon@eee.upd.edu.ph

Keywords: suitability analysis, heuristic algorithm, node allocation, air quality, low-cost sensors

Abstract

Air pollution poses significant environmental and public health risks, particularly in urban areas of low and middle-income countries like the Philippines. Regulatory air quality monitoring stations, while accurate, are expensive and limited in spatial coverage, highlighting the need for low-cost IoT-based sensor networks to provide broader and real-time air quality data. This study establishes a methodology using Geographic Information Systems (GIS) and a heuristic algorithm to determine locations for deploying low-cost IoT-based air quality sensors in urban environments, focusing on near-road areas in Quezon City. Using multi-criteria analysis, Street Aspect Ratio (SAR), traffic emissions, Global Horizontal Irradiance (GHI), and road proximity were combined to produce a suitability map; scores ranged from 0 to 6. The algorithm then selected sensor locations by combining suitability and population rasters while enforcing a minimum spacing between nodes. In a 40-sensor test, the resulting networks covered approximately 1.27 - 1.35 million residents (23.0%–24.4% of the city's population) across weighting schemes while maintaining balanced spatial dispersion. These results indicate that the method achieves substantial population coverage in high-exposure corridors and aligns with public-health priorities. The framework is reproducible for other cities to enhance near-road air quality monitoring and management.

1. Introduction

Air pollution, as defined by the WHO, is the contamination of the atmosphere by harmful aerosols and gases such as PM2.5, which are linked to respiratory and cardiovascular diseases. The WHO estimates that 99% of the global population breathes air exceeding safe limits, with urban and low- to middle-income regions like the Philippines most affected. According to IQAir (2022), the country recorded an average PM2.5 concentration of 14.9 μg/m³.

Monitoring air quality is essential, but in the Philippines, regulatory stations maintained by the Environmental Management Bureau (EMB) are costly and concentrated in Metro Manila. Each occupies about 5 m² and costs $15,000–$40,000 (₱878,000–₱2.34 million) to establish and maintain, requiring skilled staff and controlled environments. Consequently, only 45% of the population lives within 25 km of a monitoring site (Greenpeace, 2023), leaving large areas without consistent data.
To address this, the UP CARE project aims to complement regulatory stations with low-cost IoT-based sensors costing around ₱50,000 each (UP CARE, 2021). While less precise, these sensors improve spatial density and reveal finer air-quality variations across the city. However, current siting guidelines remain general. Both the U.S. EPA and the DENR recommend placing sensors within 20–100 m of roads, at heights of 2–15 m, and away from intersections and obstructions to ensure adequate airflow. Yet, these principles lack the specificity needed for dense urban settings, highlighting the need for context-based siting criteria tailored to near-road, low-cost sensor networks.
This study aims to develop an algorithm for designing a low-cost air quality sensor network by identifying key factors that influence sensor placement in urban areas. These factors serve as parameters for a suitability assessment using Geographic Information Systems (GIS), which determines locations for sensor deployment. The resulting suitability map provides the foundation for the algorithm to generate a sensor distribution plan that ensures broad spatial coverage, especially in near-road and high-exposure areas. By integrating technical and population-centered considerations, the study establishes a network design framework that not only improves the spatial density of air quality monitoring but also addresses the needs of local populations. Ultimately, this approach facilitates the strategic deployment of low-cost IoT-based sensors, contributing to more responsive, and effective air quality monitoring in the Philippines. Specifically, this study aims to: (1) identify siting criteria relevant to near-road deployment of low-cost IoT air quality sensors; (2) integrate Street Aspect Ratio (SAR), traffic-related emissions, global horizontal irradiance (GHI), and road proximity in a GIS-based suitability analysis to produce a suitability map; (3) develop a heuristic algorithm that uses the suitability surface and population data to generate well-spaced candidate sensor locations; and (4) demonstrate the framework in Quezon City.

Quezon City was selected as the study site because of its large population and high traffic congestion. This study is subject to several limitations. The suitability analysis is constrained to four main criteria: street aspect ratio, traffic-related emissions, road proximity, and solar radiation, excluding other possible parameters due to data and time constraints. The data used are limited to the most recent datasets provided by key agencies. Physical deployment of sensors is not within the study's scope due to budget and logistical limitations. The site selection also focuses solely on horizontal spatial positioning and does not consider vertical placement, such as sensor height above ground level.

This contribution has been peer-reviewed. The double-blind peer-review was conducted on the basis of the full paper.
https://doi.org/10.5194/isprs-annals-X-5-W4-2025-315-2026

2. Methods

The methodology is structured into seven processes: generating a LoD1 3D urban model; calculating traffic emissions per road segment using EMB emission factors; classifying road segments by flow regimes through Street Aspect Ratio; generating a solar radiation map; performing a site suitability analysis that integrates these outputs to identify appropriate near-road sensor locations; a proximity analysis; and developing an algorithm that uses the suitability map and population as inputs to design the sensor network and produce the final installation map

2.1 Data Gathering and Preparation

The study utilizes LiDAR and GIS datasets for 3D urban modeling, street geometry analysis, and solar exposure computation. Key datasets include the LiDAR DTM and DSM, as well as 2D features such as building footprints and road networks from OpenStreetMap. Traffic volume and emission factor data are used for the calculation of PM2.5 emissions, while population data from the WorldPop dataset accessed through GEE is used to generate a population density map. Table 1 provides an overview of these datasets, their sources, and spatial resolutions.

Data Set	Specification	Source
Terrain Models		
Digital Terrain Model (DTM)	1 × 1 m.	Project LiPAD (DOTr, 2021)
Digital Surface Model (DSM)	1 × 1 m.	Project LiPAD (DOTr, 2021)
2D Feature		
Building Footprint	—	OpenStreetMap
Road Network	—	OpenStreetMap
Traffic Data		
Annual Average Traffic Data	Circumferential and Radial Roads	MMDA (through FOI)
Emission Factor Data	—	Vergel & Tiglao (2013)
Population Data	100 × 100 m	Google Earth Engine

Table 1. Summary of Data Sets Used

The LiDAR-derived Digital Terrain Model (DTM) and Digital Surface Model (DSM), each with a 1×1 m resolution, represent bare ground and surface elevations, respectively, and support 3D modeling of the study area. 2D features were extracted from OpenStreetMap using the QuickOSM plugin in QGIS (Dupuy, 2017). Roads and buildings were retrieved per 2500×2500 m grid and merged into a single vector layer. Annual Average Daily Traffic (AADT) data from MMDA (2023) provided average vehicle counts by type on major roads. Vehicle emissions were estimated using EMB's emission factors, which relate pollutant output to vehicle type and travel distance. Sensor placement prioritizes densely populated areas, using 100×100 m gridded population data obtained from the WorldPop dataset (WorldPop, 2020) accessed through the Google Earth Engine platform. This ensures sensor coverage aligns with population distribution in Quezon City.

2.2 3D Urban Model

The 3D Urban Model for Quezon City was generated using LiDAR DSM and DTM, along with building footprint and road network data. Building heights were estimated using a Normalized Digital Surface Model (nDSM), derived by subtracting ground elevation (DTM) from surface elevation (DSM). These heights were then used to extrude 3D buildings by integrating the building footprints with nDSM (Fattoruso et al., 2020; Lastrollo, 2019). The resulting model corresponds to Level of Detail 1 (LoD1), which represents buildings as simple block models without roof structures or façade details. While generalized, this level of detail is sufficient for calculating the Street Aspect Ratio (SAR), making the 3D Urban Model an essential component of the study.

2.3 Traffic Emission Calculation

In this study, road segments were assigned traffic volumes based on their classification as primary, secondary, or tertiary, following the Department of Public Works and Highways (DPWH) guidelines. The OpenStreetMap (OSM) road network was manually reclassified accordingly. Traffic data was limited to Annual Average Daily Traffic (AADT) figures for 2023, sourced from the DPWH. Three representative roads were selected: EDSA (primary), Quezon Avenue (secondary), and C.P. Garcia (tertiary), to represent each category. Their traffic volumes were used as an approximation for all roads of the same classification in Quezon City due to data limitations. This assumes that traffic patterns and fleet compositions from the sampled roads are representative of other roads in the same class, even though actual conditions may differ.

Emission rates were calculated using the formula:

$$E_v = \sum_i (v_i d_i)\, EF_i \quad (1)$$

where E_v = total emissions per day (mass)
v_i= number of vehicles of category i
d_i = distance traveled by vehicles of category i (km)
EF_i= emission factor for vehicle category i (g/km)

The equation was used to compute total emissions per road segment using vehicle volume, assumed travel distance, and emission factors. The travel distance for each vehicle category was assumed to be equal to the road length of each segment, without accounting for variations caused by stop-and-go traffic or rerouting. Emission factors from UP NCTS (Vergel and Tiglao, 2013), which vary by vehicle type and speed, were assigned to each segment based on speed limits of their respective road classes. This assumes that vehicles generally operate at or near the prescribed speed limits, even though congestion often results in lower average speeds.

It is important to note that the DPWH AADT (2023) dataset only provides traffic counts for selected major roads and not for the entire road network of Quezon City. Thus, the estimates represent average daily flows and do not capture temporal variations such as peak versus off-peak conditions or seasonal fluctuations. Likewise, the dataset may not fully represent the actual mix of vehicles across all road segments, especially on smaller or local roads where informal transport modes are more common. These assumptions, particularly the use of uniform traffic volumes across road classes and representative roads, as well as the exclusion of congestion patterns and hourly traffic variations, may limit the spatial variability of the traffic emission map. As a result, localized hotspots could be underrepresented, which in turn may affect suitability scores and the prioritization of specific road segments for sensor deployment.

2.4 Street Aspect Ratio Identification

The Street Aspect Ratio (SAR), defined as the ratio of building height to street width, was calculated by generating points along the road network shapefile at 5-meter intervals. From these points, 50-meter-long transect lines perpendicular to the street segments were created. These lines were trimmed to terminate at building façades, resulting in a layer of perpendicular lines spaced every 5 meters and ending at the façades on each side of the street. The width of each street segment was then determined by averaging the lengths of the transect lines crossing it (Mohajeri et al., 2019). To calculate the average building height, the Zonal Statistics tool was used, with the road segments as zones and the normalized Digital Surface Model (nDSM) as the input raster. After determining the average building height and average street width, the SAR for each road segment was computed by dividing the average building height by the average street (or canyon) width. From a dispersion perspective, SAR is a critical determinant of near-road air pollution levels. Literature shows that low SAR values (<0.5) are associated with well-ventilated streets where pollutants disperse more easily, while moderate SAR values (≈0.5–2.0) create canyon effects that restrict airflow and lead to pollutant accumulation (Oke, 1988; Hang et al., 2012). High SAR values (>2.0) indicate deep urban canyons, where dispersion is very limited, and exposure risks are elevated (Xie et al., 2005). Thus, SAR directly reflects the extent to which urban form influences pollutant trapping. For this study, the street segments were categorized into three SAR ranges: (a) SAR < 0.33, (b) 0.33 < SAR < 0.67, and (c) SAR > 0.67 (Anselm Akubue, 2019; Hang et al., 2012). These categories allow identification of road environments that are either relatively ventilated or prone to higher pollutant concentrations. Categorizing SAR into three segments simplifies analysis and interpretation, allows clear scoring for suitability assessments, reduces sensitivity to minor variations, and makes it easier to identify suitable areas compared to using raw continuous values. In the context of this study, SAR is essential because it directly informs the suitability assessment for sensor siting. Road segments with higher SAR values indicate potential pollutant buildup, making them priority areas for monitoring, while lower SAR segments can serve as comparative baselines. Including SAR as a criterion ensures that the algorithm accounts for urban form effects on pollutant dispersion when selecting sensor locations.

2.5 Solar Radiation

The computation of sun exposure was conducted using QGIS by first generating aspect and slope rasters from the Digital Terrain Model (DTM). These layers represent the terrain's orientation and inclination, which are critical in determining solar exposure. Using these, along with the normalized Digital Surface Model (nDSM), various solar radiation parameters were calculated. These include direct incoming solar radiation and diffuse incoming solar radiation, both expressed in Wh/m², as well as the duration of direct solar exposure in hours. The process incorporated terrain analysis to derive slope and aspect and used these inputs to generate outputs such as global horizontal irradiation, direct normal irradiance, reflected radiation, and diffuse radiation.

2.6 Proximity Analysis

For near road air quality monitoring, the sensors are prioritized to be placed within 10-20 meters from the edge of the road (Baldauf et al. ,2009.; Shirato et al. ,2015). In this study, a buffer of 10 meters was made for the road network which was already assumed to be the width of the road from the center line. Hence, this assumption generalizes all the road widths in Quezon City to be 20 meters. This is in line with the Executive Order No. 621 which states that the minimum width of national roads shall be 20 meters. To model proximity zones, the initial road area layer was buffered three additional times at distances of 10, 15, and 20 meters. The Difference tool was then used to extract three distinct zones: 0–10 m, 10–15 m, and 15–20 m from the road edge. These individual buffer zones were subsequently merged into a single proximity layer to support spatial analysis.

2.7 Site Suitability

The suitability analysis combined four geospatial variables: Street Aspect Ratio (SAR), solar radiation, traffic emissions, and road proximity. These variables were scored and integrated using the Weighted Linear Addition (WLA) method, a widely used multi-criteria decision analysis method in spatial planning (Malczewski, 1999) to produce a final suitability map for low-cost IoT air quality sensor deployment.

Four criteria guided the evaluation of site suitability: (1) proximity within 20 meters from the curb, (2) high solar irradiation, (3) high SAR (> 0.67), and (4) high traffic emissions. Each factor was reclassified into three suitability levels: low, moder- ate, and high, corresponding to scores of 0, 1, and 2. For SAR, segments > 0.67 scored 2, 0.33–0.67 scored 1, and < 0.33 scored 0 (Anselm Akubue, 2019). Traffic emission scores were based on classified pollutant concentrations, while solar radiation was reclassified using equal intervals. Road proximity was divided into three zones: 0–10 m (score 2), 10–15 m (score 1), and 15–20 m (score 0), prioritizing locations closer to roads. All vector layers were rasterized and aligned with the solar radiation raster (in terms of pixel size and extent), then combined using WLA with equal weights. This produced a preliminary suitability raster, which was then converted back to a vector layer. To refine the results, unsuitable areas, specifically parks, were excluded, as these act as pollutant sinks and are not ideal for near-road monitoring. These features were vectorized and used in a spatial difference operation to remove overlapping park areas from the suitability layer. The final out- put, a cleaned and rasterized suitability map, identifies optimal sites for deploying air quality sensors near roads while avoiding green spaces that could skew pollutant readings.

2.8 Node Deployment Algorithm

The node deployment algorithm was developed to place a specified number of sensors within a defined area using suitability and population rasters, with the goal of maximizing population coverage in highly suitable locations while maintaining a minimum distance between sensors. A GUI built with Tkinter (Lundh, 1999) allowed users to input sensor count and select input rasters. Upon initiation, the algorithm used rasterio (Gillies et al., 2013) to read the data and convert them into NumPy arrays (Harris et al., 2020). These were combined into weighted scores, favoring locations with both high suitability and population density.

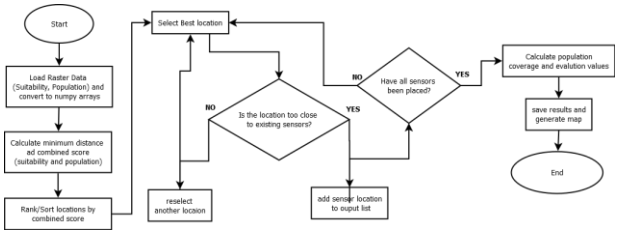

Figure 1. Heuristic Sensor Placement Algorithm

Figure 1 shows the flowchart of the heuristic sensor placement algorithm. Each pixel was scored as the sum of its suitability and population values. The algorithm then sorted these scores in descending order and placed sensors iteratively at the highest-scoring locations that met the minimum distance requirement. This constraint ensured spatial dispersion and avoided overlapping coverage.

To implement the distance requirement, a decay constant was calculated using the average area coverage per node (A_{node}), sensor range (r), and the minimum distance between nodes (r_{min}), following the method of Dolar and Medrano (2023). The distance $r2$, derived using an exponential decay function, represents the point where the citizen satisfaction score drops to 0.5. The minimum sensor spacing was computed using the study area's total size and the number of sensors, ensuring non-overlapping yet extensive coverage.

The equations used to compute the minimum distance between sensor nodes are shown below:

$$A_{node} = \frac{A_{total}}{\#\ of\ nodes} \quad (2)$$

where A_{node} = average area covered by one node (m²)
A_{total} = total study area (m²)
$\#\ of\ nodes$ = number of sensor nodes (dimensionless)

$$r = \sqrt{\frac{A_{node}}{\pi}} \quad (3)$$

where A_{node} = average area covered by one node (m²)

r = equivalent radius of the area covered by one node (m)

$$\theta = \frac{-r}{ln(0.1)} \quad (4)$$

where θ = decay constant
r = equivalent radius of the area covered by one node (m)

$$r_2 = ln(0.5) \cdot \lambda \quad (5)$$

where θ = decay constant
r_2 = where the citizen satisfaction score drops to 0.5

$$r_{min} = 2 \cdot r_2 \quad (6)$$

where r_2 = where the citizen satisfaction score drops to 0.5
r_{min} = minimum recommended spacing between sensor nodes (m).

These equations define the spatial influence of each sensor and ensure non-overlapping coverage. For each sensor placed, the algorithm computed the population within its coverage radius by summing the raster values. Overlapping population was avoided by tracking covered cells. This process continued until all sensors were placed optimally. After placement, a map was generated showing sensor locations and coverage areas, with labels for each sensor. The algorithm also evaluated network performance through population coverage efficiency, average and minimum inter-sensor distances, and spatial autocorrelation using Moran's I, implemented via the esda and libpysal libraries.

The coverage efficiency of the sensor network was assessed by calculating the percentage of the total population within the sensors' coverage areas. This ensured that sensor placement prioritized densely populated regions. To evaluate spatial distribution, the average distance between all sensor pairs was calculated, confirming that sensors were neither too clustered nor too far apart. The minimum distance between any two sensors was also measured to avoid redundant placement and overlapping coverage. Additionally, the spatial pattern of sensor deployment was analyzed using Moran's I statistic, which quantified the degree of clustering or dispersion. A corresponding p-value was calculated to assess the statistical significance of the observed pat- tern, ensuring that the network was strategically distributed for effective air quality monitoring.

3. Discussion

3.1 Street Aspect Geometry Identification

The results showed that most national road segments in Quezon City had a street aspect ratio of < 0.33, indicative of *isolated roughness flow* (Oke, 1988; Grimmond & Oke, 1999), typically found in areas with open spaces and low-rise buildings. These conditions promote better air circulation and pollutant dispersion, reducing the likelihood of air quality issues.

Figure 2. Street segments exhibiting *skimming flow* based on Street Aspect Ratio (SAR) overlaid on Google Earth imagery (Google Earth, 2024) (from left to right): Araneta, Cubao & Eastwood City.

Figure 2 identifies segments of Aurora Boulevard, General Aguinaldo Avenue (near Araneta Cubao Station), and Eastwood Avenue and Richmond Road (in Eastwood City) with street aspect ratios above 0.67, indicating *skimming flow*. This flow type reflects poor pollutant dispersion caused by tall buildings and narrow streets that limit airflow. Structures like the 135-meter-tall Manhattan Parkway Towers and the LRT Araneta Cubao Station contribute to pollutant buildup in Araneta Cubao. Eastwood City shows some of the highest SAR values, especially on Eastwood Avenue (1.033) and Richmond Road (1.149). Eastwood Avenue is lined by tall structures like Eastwood Palazzo Residence, Excelsior, and Eastwood Mall, which limit air circulation. Richmond Road is bordered by buildings such as One Orchard Road Condominium and Olympic Heights,

elevating SAR and indicating a strong tendency for pollutant retention.

Figure 3 identifies street segments with *wake interference flow*, marked by moderate pollutant dispersion due to interactions between building height and street width that generate turbulent airflows. These segments are mostly located in previously identified skimming flow areas, with additional ones along EDSA (near Kamuning and North Avenue Stations) and in Ortigas (Poveda Street and ADB Avenue).

Figure 3. Street segments exhibiting *wake interference flow* based on Street Aspect Ratio (SAR) layers, overlaid on Google Earth imagery (Google Earth, 2024) (from left to right): North Avenue Station (EDSA), Kamuning Station (EDSA), Eastwood City, Araneta Cubao, Ortigas (Poveda Street) & Ortigas (ADB Avenue)

In EDSA, MRT-3 North Avenue and GMA Kamuning Stations are likely contributors to wake interference. Araneta Cubao, with SAR values ranging from 0.332 to 0.661, shows the most significant interference, intensified by structures like MRT and LRT Cubao Stations, Gateway Mall, and Smart Araneta Coliseum. Eastwood City segments such as Eastwood Avenue, Orchard Road, and E-Commerce Avenue exhibit moderate SAR values (0.354–0.571). High-rises like One Lafayette, One Eastwood Avenue Towers, IBM Plaza, and Citibank Square influence air- flow, though relatively wider streets help moderate pollutant buildup. In Ortigas, Poveda Street and ADB Avenue have the lowest SAR values (0.334–0.349), due to wider roads and moderate building heights. Structures like Robinson's Galleria, Saint Pedro Poveda College, and Crowne Plaza Manila allow for better air circulation. Adjacent but outside the study area, high-rise buildings along ADB Avenue, such as Holiday Inn Manila Galleria and AIC Empire Tower, may still affect local air quality and should be considered in future studies.

3.2 Solar Radiation

The photovoltaic potential of a location depends on factors such as solar position, angle of incidence, and day of the year. In this study, weather conditions were excluded, as solar radiation was computed using the r.sun module in GRASS GIS, which assumes clear-sky conditions (Scharmer and Greif, 2000; Page et al., 2001; Rigollier, 2001).

The GHI in the study area ranged from approximately 432 to 1215 Wh/m^2/day, which is sufficient to power low-cost IoT-based air sensors. The spatial distribution of solar radiation followed terrain patterns, reflecting the influence of nDSM, aspect, and slope data. To integrate solar potential into the suitability analysis, the GHI output was reclassified into three categories: 0 (least suitable, 400–700 Wh/m^2/day), 1 (moderately suitable, 700–1000Wh/m^2/day)and 2 (most suitable(> 1000 Wh/m^2/day)

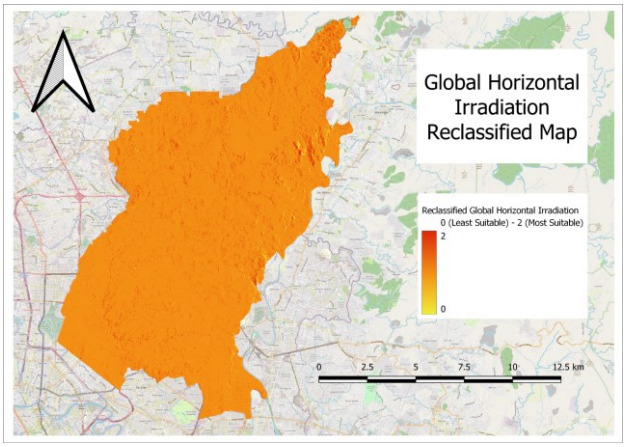

Figure 4. Reclassified GHI Map

Although r.sun is open-source and accessible, it is computationally intensive. Thus, the solar radiation was calculated only once, using the Winter Solstice as the Julian date to represent minimal solar conditions. The typical method of averaging seasonal values was not applied, which may be a limitation of this study.

3.3 Traffic Emission Calculation

The pollutant of interest in this study is PM or particulate matter, so the methodology to estimate the traffic emission is specific to this pollutant.

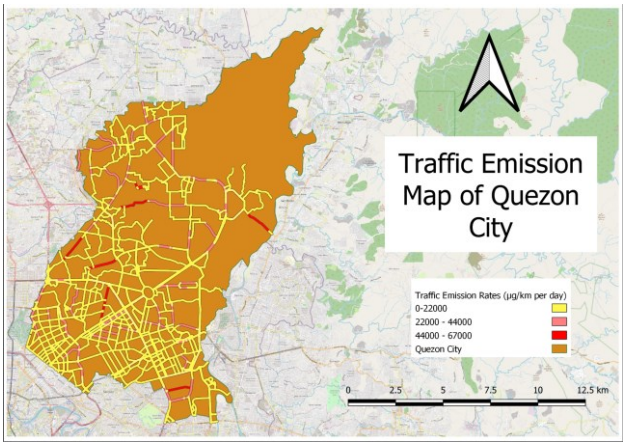

Figure 5. Traffic Emission Map of Quezon City

In Figure 5, the traffic emission map is divided into three categories of equal intervals, based on the values obtained from the estimation process. The figure illustrates that the majority of roads fall within the 0–22,000 μg/km per day category, with only a few roads falling within the 44,000–67,000 μg/km per day

category. As most roads are categorized similarly, the resulting traffic emissions map displays limited spatial variability.
This study includes several assumptions regarding traffic emission estimation, such as the uniform traffic volume across different road categories and the constancy of traffic conditions. Additionally, meteorological factors like temperature, wind speed, and wind direction, which influence the dispersion of traffic emissions, were not considered in this study. These factors represent potential limitations in the methodology of traffic emissions estimation.

3.4 Suitability Analysis

The preparation of layers for the suitability analysis is a critical aspect of this study. It was essential that all required layers shared a consistent coordinate system. In this case, the PRS 92 coordinate system was chosen to be used. Additionally, the rasterization of vector layers was conducted to ensure alignment with the raster layers for the Weighted Linear Addition (WLA). The suitability analysis serves as the integrative process for all layers, ensuring that each parameter is considered to accurately identify the most suitable sites. In this study, the suitability analysis can yield large areas for potential sites, and these will be taken as the input for the algorithm. Figure 6 below shows the suitability map of Quezon City for low-cost IoT-based air quality sensors.

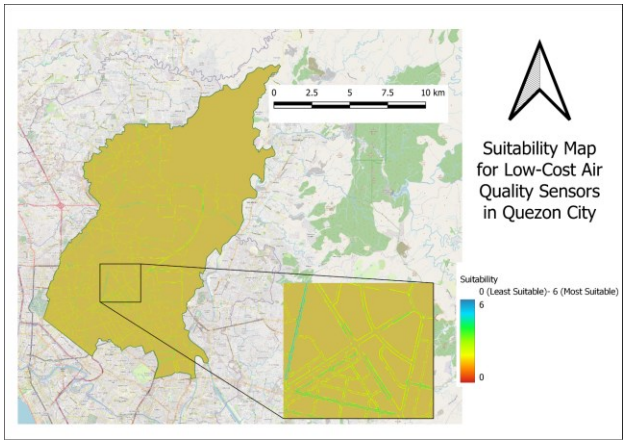

Figure 6. Suitability Map of Low-Cost Air Quality Sensors in Quezon City

Figure 6 shows the range of the suitability scores goes from 0 to 6, with 0 assigned to areas being the least suitable while 6 assigned to areas being the most suitable. However, one thing to note is that the actual theoretical maximum of the suitability rating is 8 since there were 4 parameters considered: SAR, Traffic Emission, Road Proximity, and Solar Irradiation, each having a maximum score of 2. These four criteria were selected under the hypothesis that they represent both exposure risk and operational feasibility: SAR and traffic emissions capture urban form and pollutant sources affecting concentration levels, while road proximity ensures alignment with near-road monitoring standards, and solar irradiance provides the basis for continuous solar-powered sensor operation.

A possible reason for the reduced maximum observed is that during the WLA process, a pair of factors were not able to reach the maximum possible value simultaneously, wherein only one of them was highly suitable. The suitability assessment was conducted using four pre-selected criteria: Street Aspect Ratio, traffic-related emissions, road proximity, and Global Horizontal Irradiance, and areas of tree cover were not accounted for, which can be a limitation of this study; the only areas that were subtracted from the suitable areas were some parks which could act as pollution sinks due to the abundance of vegetation in these areas.

To enable citywide analysis despite data gaps, assumptions on traffic emissions and generalized road widths were applied. These simplifications allowed implementation but introduced uncertainty that may affect suitability scores and spatial variability in dense areas like Quezon City. Since the placement algorithm depends on these indicators, this uncertainty could influence both the results and the network evaluation. Nevertheless, the analysis identified areas where sensors can effectively capture pollutant exposure and support emission control planning. Future work may include additional factors such as tree cover, meteorology, and land use to improve site prioritization.

3.5 Node Deployment Algorithm

The algorithm workflow incorporates both the 20 existing and 20 additional LGU-operated sensors to form a 40-sensor network. While no reference-grade PM measurements were available for validation, the algorithm relies on spatial indicators: traffic emissions, Street Aspect Ratio (SAR), road proximity, and solar irradiance, to identify high-exposure areas for monitoring.

Several weight configurations were tested to evaluate the impact of prioritizing suitability and population. The weights assigned to population (β) and suitability (α) were varied across runs. The initial run used equal weights ($\alpha = 0.5$, $\beta = 0.5$). In subsequent runs, the population weight β was gradually increased from 0.6 to 0.9, while the suitability weight α decreased from 0.4 to 0.1. Several sensors remain in the same locations across multiple beta weight configurations, indicating that the algorithm consistently identifies them as optimal. For instance, Sensors 1 and 2 retain their positions and scores at beta weights 0.5, 0.6, and 0.7. Sensor 1 maintains a population coverage of 6,148 and a suitability score of 6, while Sensor 2 covers 40,818 with the same suitability score, highlighting their importance in balancing coverage and suitability. As the population weight (β) increased from 0.5 to 0.9, the number of sensors in highly suitable locations (score of 6) declined from 7 to 4. Similarly, sensors in moderately suitable areas (score of 5) dropped from 21 to 13. This trend reflects the algorithm's growing emphasis on population coverage as β increases. Conversely, more sensors were placed in lower suit- ability areas. Sensors with a score of 4 rose from 12 at $\beta = 0.5$ to 19 at $\beta = 0.9$, and two sensors even had a score of 3 at the highest β value. This reflects the algorithm's shift toward prioritizing population coverage over site suitability. Some sensors consistently cover fewer people due to their placement in less populated areas, but they help maintain spatial balance in the network. For example, Sensor 7 at $\beta = 0.5$ covers 5,346 individuals but has a high suitability score of 6. Located along Maharlika Highway near the EDSA People Power Monument, its placement is justified by high traffic emissions in the area, including nearby P. Santos and White Plains Avenues. This location is reused for Sensor 9 at $\beta = 0.6$, Sensor 18 at $\beta = 0.7$, and Sensor 25 at $\beta = 0.8$.

As population weight (β) increases, some high-suitability but low-population areas are excluded from sensor placement. This highlights a trade-off between spatial coverage and population

density. The shift shows the algorithm's sensitivity to β: sensors in emission-heavy, sparsely populated areas lose priority as denser zones are favored, though they remain critical at lower β values for monitoring key emission sources.

3.6 Sensor Network Evaluation

Metric	$\alpha = 0.5$ $\beta = 0.5$	$\alpha = 0.4$ $\beta = 0.6$	$\alpha = 0.3$ $\beta = 0.7$	$\alpha = 0.2$ $\beta = 0.8$	$\alpha = 0.1$ $\beta = 0.9$
Total Covered Population	1,268,830	1,281,267	1,280,790	1,322,396	1,346,671
Coverage Efficiency	23.00%	23.23%	23.22%	23.97%	24.41%
Average Distance Between Sensors	6936.39	6913.72	6790.36	7003.94	6933.63
Minimum Distance Between Sensors	1394.52	1394.52	1394.52	1394.52	1400.37
Moran's I	0.0759	0.0682	0.1173	0.0090	-0.0499
p-value	0.2660	0.2820	0.2350	0.4260	0.4450

Table 2. Evaluation Values of Different Weight Configurations

Table 2 shows how evaluation values change with different alpha and beta weights. As beta increases, shifting focus toward population, the total covered population rises from 1,268,830 ($\beta = 0.5$) to 1,341,671 ($\beta = 0.9$), with coverage efficiency increasing from 23.00% to 24.41%. Average and minimum distances between sensors remain relatively stable, indicating compact but evenly spaced placements. Spatial autocorrelation (Moran's I) ranges from slight clustering (0.1173 at $\beta = 0.7$) to slight dispersion (−0.0499 at $\beta = 0.9$), though none are statistically significant ($p > 0.05$). Overall, increasing beta improves population coverage while maintaining balanced sensor distribution.

3.7 Manual Validation

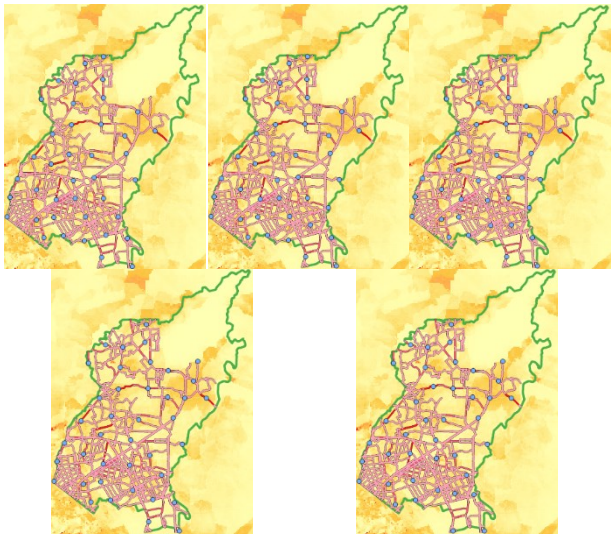

Figure 7. Different weight configurations for sensor placement overlay on population and traffic emission layers (from left to right): α = 0.5, β = 0.5; α = 0.4, β = 0.6; α = 0.3, β = 0.7; α = 0.2, β = 0.8; and α = 0.1, β = 0.9.

Figure 7 shows sensor placements across different weight configurations overlaid on population and traffic emission layers. Changes in weight settings had subtle effects, indicating consistent algorithm performance. In all cases, over half of the sensors were near moderate to high traffic emission zones. At $\alpha = 0.5$, $\beta = 0.5$, there were 38 such placements, decreasing to 36, 30, 31, and 26 as α decreased to 0.4, 0.3, 0.2, and 0.1. The slight rise at $\alpha = 0.2$ may be due to high SAR values maintaining site suitability. Even at the lowest α, sensors still clustered around emission hotspots, showing that suitability remained a key factor. Some sensors also overlapped with both high-emission and high-population areas.

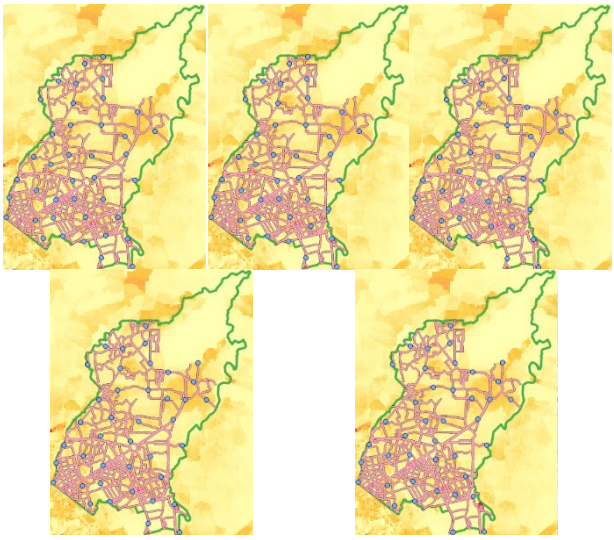

Figure 8. Different Weight Configurations for Sensor Placement Overlaid on Population Density and SAR layers (from left to right): α = 0.5, β = 0.5; α = 0.4, β = 0.6; α = 0.3, β = 0.7; α = 0.2, β = 0.8; and α = 0.1, β = 0.9.

Figure 8 shows sensor placements overlaid on population density and SAR layers across different weight configurations. Only one sensor was consistently placed in a high SAR area, initially near Orchard Road ($\alpha = 0.5$ to 0.4) and later shifting to Poveda Street ($\alpha = 0.1$), suggesting a shift to maximize population coverage. While some sensor locations remained fixed, others showed minor adjustments.

4. Conclusion

This study developed a methodology for siting low-cost IoT-based air quality sensors in urban near-road environments. Four criteria: Street Aspect Ratio (SAR), traffic emissions, global horizontal irradiance (GHI), and road proximity, were integrated into a GIS-based suitability analysis to produce a suitability map. A heuristic algorithm was then applied to generate sensor locations using both suitability scores and population distribution. The findings show that SAR identifies road segments prone to pollutant buildup, traffic emissions highlight primary exposure sources, GHI ensures the feasibility of solar-powered operation, and road proximity captures near-road exposure. The algorithm produced a well-distributed set of candidate sensor sites in Quezon City, offering improved coverage compared to the limited placement of regulatory stations. This demonstrates that integrating geospatial criteria with population data provides a practical methodology for designing sustainable, exposure-focused air quality sensor networks. While applied in Quezon City, the methodology can

be adapted to other urban areas facing similar monitoring challenges.

The methodology is constrained by data limitations. The use of uniform traffic emission assumptions and generalized road widths, while necessary to enable citywide analysis, may have reduced spatial variability and affected the resulting suitability scores. Future research should incorporate more detailed traffic information, actual road dimensions, and meteorological parameters to enhance the accuracy of exposure assessment and optimize sensor placement. Physical deployment and long-term validation are also recommended to evaluate real-world performance. Moreover, subsequent studies may examine vertical siting considerations, integration with mobile or satellite-based measurements, and the application of the methodology to other urban contexts to assess its transferability.

References

Anselm Akubue, J., 2019. Effects of street geometry on airflow regimes for natural ventilation in three different street configurations in Enugu City. Different Strategies of Housing Design.

Baldauf, R., Watkins, N., Heist, D., Bailey, C., Rowley, P., Shores, R., 2009. Near-road air quality monitoring: Factors affecting network design and interpretation of data. Air Quality, Atmosphere & Health, 2(1), 1–9. doi.org/10.1007/s11869-009-0028-0.

Biljecki, F., Ledoux, H., Stoter, J., 2016. An improved LOD specification for 3D building models. Computers, Environment and Urban Systems, 59, 25–37. doi.org/10.1016/j.compenvurbsys.2016.04.005.

Brzozowski, K., Ryguła, A., Maczynski, A., 2019. The use of low-cost sensors for air-quality analysis in road intersections. Transportation Research Part D: Transport and Environment, 77, 198–211. doi.org/10.1016/j.trd.2019.10.019.

Dolar, P.A., Medrano, H.M., 2023. Developing a neighborhood-scale LoRa-based $PM_{2.5}$ air-quality sensor network. (Unpublished manuscript.)

Fattoruso, G., Nocerino, M., Toscano, D., Pariota, L., Sorrentino, G., Manna, V., De Vito, S., Cartenì, A., Fabbricino, M., Di Francia, G., 2020. Site suitability analysis for low-cost sensor networks for urban spatially dense air-pollution monitoring. Atmosphere, 11(11), 1215. doi.org/10.3390/atmos11111215.

Gago-Silva, A., 2016. GRASS GIS in grid environment. doi.org/10.6084/m9.figshare.3188950.

Google Earth, 2024. Google Earth Pro. (Accessed 11 August 2024) earth.google.com.

GRASS Development Team, 2017. Geographic Resources Analysis Support System (GRASS) Software. Open Source Geospatial Foundation. grass.osgeo.org (20 September 2017).

Hang, J., Li, Y., Sandberg, M., Buccolieri, R., Di Sabatino, S., 2012. The influence of building-height variability on pollutant dispersion and pedestrian ventilation in idealized high-rise urban areas. Building and Environment, 56, 346–360. doi.org/10.1016/j.buildenv.2012.03.023.

Harris, C.R., Millman, K.J., van der Walt, S.J., Gommers, R., Virtanen, P., Cournapeau, D., Oliphant, T.E., 2020. Array programming with NumPy. Nature, 585, 357–362. doi.org/10.1038/s41586-020-2649-2.

IQAir, 2022. 2022 World Air Quality Report. IQAir, Switzerland.

Lastrollo, E.B., 2019. A CFD-based air-quality dispersion modelling for urban areas using OpenFOAM. Thesis, University of the Philippines Diliman.

Li, Y., Hoi, K.I., Mok, K.M., Yuen, K.V., 2023. Emerging air-quality monitoring methods. In: Air Quality Monitoring and Advanced Bayesian Modeling, 105–172.

Lundh, P., 1999. Multi-criteria decision analysis in GIS: A case study. Geographical and Environmental Modelling, 3(1), 65–82.

Malczewski, J., 1999. GIS and multicriteria decision analysis. John Wiley & Sons, New York.

Meng, X., Zhang, K., Pang, K., Xiang, X., 2020. Characterization of spatio-temporal distribution of vehicle emissions using web-based real-time traffic data. Science of the Total Environment, 709, 136227. doi.org/10.1016/j.scitotenv.2019.136227.

Mohajeri, N., Gudmundsson, A., Kunckler, T., Upadhyay, G., Assouline, D., Kampf, J.H., Scartezzini, J.L., 2019. A solar-based sustainable-urban design: The effects of city-scale street-canyon geometry on solar access in Geneva, Switzerland. Applied Energy, 240, 173–190. doi.org/10.1016/j.apenergy.2019.02.014.

Oke, T.R., 1988. Street design and urban-canopy-layer climate. Energy and Buildings, 11, 103–113.

Petetin, H., Subramanian, R., Robinson, A.L., Apte, J.S., 2020. Spatial representativeness of a near-road air-quality monitoring station. Environmental Science & Technology, 54(11), 7029–7038. doi.org/10.1021/acs.est.0c00362.

UP Center for Air Research and Education (UP CARE), 2021. National Emissions Inventory: Road Transport Sector. University of the Philippines Diliman.

United States Environmental Protection Agency (EPA), n.d. Air quality monitoring reference. (Accessed 23 May 2023) epa.gov.

World Health Organization (WHO), 2022. Air quality guidelines. World Health Organization, Geneva.

WorldPop, 2020. Global High-Resolution Population Denominators Project, Version 2. University of Southampton. doi.org/10.5258/SOTON/WP00647.